

Different shape models for erythrocyte: Light scattering analysis based on the discrete sources method

Elena Eremina^{a,*}, Jens Hellmers^a, Yuri Eremin^b, Thomas Wriedt^c

^a*Universitaet Bremen, Badgasteiner Str. 3, 28359 Bremen, Germany*

^b*Faculty of Applied Mathematics and Computer Science, Moscow State University, Lenin's Hills, 119992 Moscow, Russian Federation*

^c*Institut für Werkstofftechnik, Badgasteiner Str. 3, 28359 Bremen, Germany*

Abstract

In practical applications a precise and fast detection of the shape of a single erythrocyte from its scattering characteristics is needed. For this reason detailed investigations of light scattering properties of erythrocyte and their relation to shape is of great interest in recent years. In this paper we analyze light scattering behavior of different shape models of erythrocyte using the discrete sources method. For this we compare scattering results for oblate spheroid, disk-sphere, Cassini-based shape and a shape for a real strainless erythrocyte introduced by Skalak. Numerical results for the scattering indicatrix and the differential cross section by different shape models and its orientations are presented.

© 2006 Elsevier Ltd. All rights reserved.

Keywords: Erythrocyte; Light scattering; Discrete sources method

1. Introduction

Light scattering by blood cells is recently of great interest both in mathematical modeling and in practical applications. Between other blood cells, the red blood cell—erythrocyte—is the most studied in the last years, because it plays an important role in blood due to its hemoglobin content. Erythrocytes are the most numerous cells in blood and light scattering by erythrocytes promise to be an appropriate method for detection of some blood diseases. The erythrocyte has an advantage for modeling, as it has no internal structure (like nucleon) and can be modeled as a homogeneous object with a certain refractive index. On the other side light scattering simulation is difficult due to the fact that erythrocyte has a relatively large (with respect to the exciting wavelength) size, which can vary from 4 to 9 μm in diameter and its main shape characteristics: the natural shape of a strainless erythrocyte is a biconcave discoid. But the erythrocyte is surrounded by a thin elastic membrane and can change its form from biconcave to toroidal or to spherical one depending on outward conditions.

In experimental studies and medical diagnostics the precise and fast detection of the shape of erythrocytes by its light scattering is of interest. That is why there is a need for univocal interpretation of experimental

*Corresponding author. Tel: +49 421 218 3583, fax: +49 421 218 5378.

E-mail address: eremina@iwt.uni-bremen.de (E. Eremina).

results. To provide such accordance between measured scattering parameters of an erythrocyte with its shape a detailed theoretical investigation is necessary. Unfortunately light scattering simulation for biconcave shapes is not an easy task. To simplify this process often models of oblate disks and spheroids are used. In other works the erythrocyte has been modeled based on Cassini ovals, which allow taking into account concavities [1]. There also exist a variety of equations to approximate the real biconcave shape of a strainless erythrocyte [2,3]. An overview can be found in [4].

Recently different methods have been applied to analyze light scattering by a single erythrocyte: finite difference time domain (FDTD) [5,6], discrete dipole approximation (DDA) [4,6], multipole multiple technique (MMP) [7], T-matrix [8]. Some of these methods are not applicable to the real biconcave shape of erythrocyte and others are rather time consuming. Because of this the discrete sources method (DSM) [9] looks very attractive, as it allows making use of the axial symmetry of the particle and polarization of the incident excitation, which sufficiently reduces the time of computations. Besides, the DSM allows computation of scattering for all the incident angles and polarizations at once [10], which is not possible for many other methods.

This is a second paper where the DSM is applied to model erythrocyte. In the first paper [11] the most common non-concave shape models, like disk-sphere and spheroid have been compared to the Skalak model. In this paper we took a Cassini-based biconcave shape in addition to those, taken before. We also calculated the scattering indicatrix, which can be directly measured by detecting devices like scanning flow cytometer [12].

2. Theory outlines and numerical algorithm

Consider scattering in an isotropic homogeneous medium in R^3 of an electromagnetic wave by a local homogeneous penetrable obstacle D_i with a smooth boundary. Let us introduce a cylindrical coordinate system (z, θ, φ) where z is the axis of symmetry of the particle and θ_i is an incident angle with respect to z . Then the mathematical statement of the scattering problem can be formulated in the following form:

$$\nabla \times \mathbf{H}_{e,i} = ik\epsilon_{e,i}\mathbf{E}_{e,i}, \quad \nabla \times \mathbf{E}_{e,i} = -ik\mu_{e,i}\mathbf{H}_{e,i} \text{ in } D_{e,i}, \quad D_e := R_3/\overline{D}_i, \quad (1)$$

$$\mathbf{n}_P \times (\mathbf{E}_i(P) - \mathbf{E}_e(P)) = \mathbf{n}_P \times \mathbf{E}^0(P), \quad \mathbf{n}_P \times (\mathbf{H}_i - \mathbf{H}_0) = \mathbf{n}_P \times \mathbf{H}^0(P), \quad P \in \partial D \quad (2)$$

and Silver–Muller radiation condition for the scattered field at infinity.

Here $\{\mathbf{E}^0, \mathbf{H}^0\}$ is an exciting field, \mathbf{n}_P is the outward unit normal vector to ∂D , index e belongs to the external domain D_e , $k = \omega/c$, ϵ, μ are permittivity and permeability, $\text{Im } \epsilon_e, \mu_e \leq 0$ (time dependence for the fields is chosen as $\exp\{j\omega t\}$) and the particle surface is smooth enough $\partial D \subset C^{(1,\alpha)}$. Then the above boundary-value problem is uniquely solvable [13].

The DSM is based on the conception of an approximate solution. The approximate solution is constructed as a finite linear combination of discrete sources (DS): dipoles and multipoles deposited in a supplementary domain inside the particle with certain amplitudes. Usually as such a domain the axis of symmetry of the particle is used. In case of an oblate particle like erythrocyte, disk or oblate spheroid it is not always possible to use the axis of symmetry [14]. For this purpose an analytical continuation to a complex plane is constructed. More detailed information can be found in [11]. The deposition of DS in a complex plane allows reducing calculation errors and time of computations.

In case of P -polarized plane wave the exciting field accepts the following form:

$$\mathbf{E}^0 = (\mathbf{e}_x \cos \theta_0 + \mathbf{e}_z \sin \theta_0) \exp\{-jk_e(x \sin \theta_0 - z \cos \theta_0)\},$$

$$\mathbf{H}^0 = -\mathbf{e}_y \cos \theta_0 \exp\{-jk_e(x \sin \theta_0 - z \cos \theta_0)\},$$

where $k_e = k\sqrt{\epsilon_e\mu_e}$.

To take into account the polarization of the external excitation we use linear combinations of electrical and magnetic multipoles. For this special vector potentials are used. For the P -polarized wave in a cylindrical

coordinate system they can be represented as:

$$\begin{aligned} \mathbf{A}_{mn}^{1,e,i} &= \{ Y_m^{e,i}(\eta, w_n^{e,i}) \cos(m+1)\varphi; -Y_m^{e,i}(\eta, w_n^{e,i}) \sin(m+1)\varphi; 0\}, \\ \mathbf{A}_{mn}^{2,e,i} &= \{ Y_m^{e,i}(\eta, w_n^{e,i}) \sin(m+1)\varphi; Y_m^{e,i}(\eta, w_n^{e,i}) \cos(m+1)\varphi; 0\}, \\ \mathbf{A}_n^{3,e,i} &= \{0; 0; Y_0^{e,i}(\eta, w_n^{e,i})\}. \end{aligned} \quad (3)$$

Here

$$Y_m^e(\eta, w_n^e) = \frac{k_e}{i} h_m^{(2)}(k_e R_{\eta w_n^e}) \left(\frac{\rho}{R_{\eta w_n^e}} \right)^m, \quad Y_m^i(\eta, w_n^i) = j_m(k_i R_{\eta w_n^i}) \left(\frac{\rho}{R_{\eta w_n^i}} \right)^m,$$

$R_{\eta w_n^e}^2 = \rho^2 + (z - w_n^e)^2$, $\eta = (\rho, z)$, $h_m^{(2)}$ is a spherical Hankel function and j_m is a spherical Bessel function. Hence, the approximate solution for the *P*-polarized wave accepts the form:

$$\begin{aligned} \begin{pmatrix} \mathbf{E}_{e,i}^N \\ \mathbf{H}_{e,i}^N \end{pmatrix} &= \sum_{m=0}^M \sum_{n=1}^{N_m^c} \left\{ p_{mn}^{e,i} \mathbf{D}_1 \mathbf{A}_{mn}^{1,e,i} + q_{mn}^{e,i} \frac{j}{\varepsilon_\zeta} \mathbf{D}_2 \mathbf{A}_{mn}^{2,e,i} \right\} + \sum_{n=1}^{N_0^c} r_n^{e,i} \mathbf{D}_1 \mathbf{A}_n^{3,e,i}, \\ \mathbf{D}_1 &= \begin{pmatrix} \frac{j}{k\varepsilon_{e,i}\mu_{e,i}} \nabla \times \nabla \times \\ -\frac{j}{\mu_{e,i}} \nabla \times \end{pmatrix}, \quad \mathbf{D}_2 = \begin{pmatrix} \frac{1}{\varepsilon_{e,i}} \nabla \times \\ \frac{j}{k\varepsilon_{e,i}\mu_{e,i}} \nabla \times \nabla \times \end{pmatrix}. \end{aligned} \quad (4)$$

The approximation solution for the case of a *S*-polarized excitation is constructed in a similar way and has the form:

$$\begin{pmatrix} \mathbf{E}_{e,i}^N \\ \mathbf{H}_{e,i}^N \end{pmatrix} = \sum_{m=0}^M \sum_{n=1}^{N_m^c} \left\{ p_{mn}^{e,i} \mathbf{D}_1 \mathbf{A}_{mn}^{1,e,i} + q_{mn}^{e,i} \frac{j}{\varepsilon_\zeta} \mathbf{D}_2 \mathbf{A}_{mn}^{2,e,i} \right\} + \sum_{n=1}^{N_0^c} r_n^{e,i} \mathbf{D}_2 \mathbf{A}_n^{3,e,i} \quad (5)$$

More details can be found in [11].

The constructed approximate solutions (4) and (5) satisfy Maxwell equations (1) and radiation conditions for the scattered fields at infinity. The unknown vector of amplitudes of DS

$$\mathbf{p}_m = \{ p_{mn}^{e,i}, q_{mn}^{e,i}, r_n^{e,i} \}_{n=1}^{N_m^c}$$

is to be determined from the transmission conditions (2). As it was mentioned above, DS are situated in a complex plane adjoined to the symmetry axis of the particle. The approximate solutions (4) and (5) are finite linear combinations of Fourier harmonics with respect to the φ angle variable. Therefore, after resolving the plane wave excitation into Fourier series with respect to the φ angle we reduce the two-dimensional approximation problem enforced at the particle surface to a set of one-dimensional problems at the particle generatrix. For solving these problems the general matching-point technique is applied, more details can be found in [15].

The exactness of the result is provided by stabilization of the scattering diagram and a posterior residual calculation.

After DS amplitudes have been determined the far-field pattern $\mathbf{F}(\theta, \varphi)$ can be computed as

$$\frac{\mathbf{E}(\mathbf{r})}{|\mathbf{E}^0(\mathbf{r})|} = \frac{\exp(-jk_e r)}{r} \mathbf{F}(\theta, \varphi) + o\left(\frac{1}{r}\right), \quad r \rightarrow \infty.$$

The components of the vector $\mathbf{F}(\theta, \varphi)$ on the unit sphere can be determined as

$$\mathbf{F}(\theta, \varphi) = \boldsymbol{\theta} F_\theta(\theta, \varphi) + \boldsymbol{\varphi} F_\varphi(\theta, \varphi).$$

Using an asymptotic representation for a P -polarized excitation the components of the far-field pattern accept the following forms:

$$\begin{aligned}
 F_{\theta}^P(\theta, \varphi) &= F^{PP} = \sum_{m=0}^M A_m(\theta) \cos(m+1)\varphi - A_0(\theta), \\
 F_{\varphi}^P(\theta, \varphi) &= F^{PS} = \sum_{m=0}^M B_m(\theta) \sin(m+1)\varphi, \\
 F_{\theta}^S(\theta, \varphi) &= F^{SP} = \sum_{m=0}^M C_m(\theta) \sin(m+1)\varphi, \\
 F_{\varphi}^S(\theta, \varphi) &= F^{SS} = \sum_{m=0}^M D_m(\theta) \cos(m+1)\varphi + A_0(\theta).
 \end{aligned} \tag{6}$$

where

$$\begin{aligned}
 A_m(\theta) &= j \sum_{m=0}^M (j \cos(\theta))^m \sum_{n=1}^{N_e^m} \{p_{mn}^e \cos \theta + q_{mn}^e\} \exp\{-jk_e z_n \cos \theta\}, \\
 A_0(\theta) &= j \sin \theta \sum_{n=1}^{N_e^0} r_n^e \exp\{-jk_e z_n \cos \theta\}, \\
 B_m(\theta) &= -j \sum_{m=0}^M (j \cos(\theta))^m \sum_{n=1}^{N_e^m} \{p_{mn}^e + q_{mn}^e \cos \theta\} \exp\{-jk_e z_n \cos \theta\}, \\
 C_m(\theta) &= j \sum_{m=0}^M (j \cos(\theta))^m \sum_{n=1}^{N_e^m} \{p_{mn}^e \cos \theta - q_{mn}^e\} \exp\{-jk_e z_n \cos \theta\}, \\
 D_m(\theta) &= -j \sum_{m=0}^M (j \cos(\theta))^m \sum_{n=1}^{N_e^m} \{p_{mn}^e - q_{mn}^e \cos \theta\} \exp\{-jk_e z_n \cos \theta\}.
 \end{aligned} \tag{7}$$

For experimental studies of blood cells scanning flow cytometers (SCF) are used. The SCF permits measurements of the angular dependency of light scattering intensity in an angle range from 5° to 100° . The design and basic principles of the SCF are described in [12]. The output signal of the SCF is proportional to the following combination of Mueller matrix elements [16]:

$$I_s(\theta) = \int_0^{2\pi} (S_{11}(\theta, \varphi) + S_{14}(\theta, \varphi)) d\varphi. \tag{8}$$

The Mueller matrix elements are connected with far-field pattern elements (6) in the following way [17]:

$$S_{14} = \text{Im}(F^{PP} F^{PS*} - F^{SS} F^{SP*}), \quad S_{11} = \frac{1}{2}(I^{PP} + I^{PS} + I^{SS} + I^{SP}), \tag{9}$$

where

$$\begin{aligned}
 I^{PP} &= \int_0^{2\pi} F^{PP} F^{PP*} d\varphi = \pi \sum_{m=0}^M |A_m(\theta)|^2 + 2\pi |A_0(\theta)|^2, & I^{PS} &= \pi \sum_{m=0}^M |B_m(\theta)|^2, \\
 I^{SS} &= \pi \sum_{m=0}^M |D_m(\theta)|^2 + 2\pi |A_0(\theta)|^2, & I^{SP} &= \pi \sum_{m=0}^M |C_m(\theta)|^2.
 \end{aligned} \tag{10}$$

Due to the axial symmetry of erythrocyte $\int_0^{2\pi} S_{14} d\varphi = 0$. Taking into account representations (9) and (10) one can write (8) as

$$I_s(\theta) = \frac{\pi}{2} \left\{ \sum_{m=0}^M (|A_m(\theta)|^2 + |B_m(\theta)|^2 + |C_m(\theta)|^2 + |D_m(\theta)|^2) \right\} + \pi |A_0(\theta)|^2. \tag{11}$$

Hence, the scattering indicatrix (11) can be easily computed as a combination of elementary functions.

Another important light scattering characteristic we consider in our paper is the differential scattering cross section (DSC), which can be calculated on the base of far-field pattern components (6) as follow:

$$\text{DSC}^{P,S} = |F_{\theta}^{P,S}(\theta, \varphi)|^2 + |F_{\varphi}^{P,S}(\theta, \varphi)|^2. \quad (12)$$

3. Numerical results

In this paper the DSM is applied to investigate the influence of different erythrocyte shape models (Fig. 1) on light scattering results. For this we choose two simple erythrocyte shape models: oblate spheroid and disk-sphere and compare them to the specific equation of erythrocyte by Skalak [2]:

$$z^2 = \left(0.86 \frac{d}{2}\right)^2 \left(1 - \left(\frac{2x}{d}\right)^2\right) \left[0.01384083 + 0.2842917 \left(\frac{2x}{d}\right)^2 + 0.01306932 \left(\frac{2x}{d}\right)^4\right].$$

Additionally we investigate a Cassini oval based shape [18]:

$$z = \pm c(-a^2 - x^2 \pm (4x^2 a^2 + b^4)^{1/2})^{1/2},$$

here c is an additional factor to manipulate the thickness of the two-dimensional shape directly. We set: $a = 2.2$, $b = 2.25$ and $c = 0.66$, the result is a biconcave shape with a diameter of $6.3 \mu\text{m}$ and aspect ratio of approximately 4:1 (Fig. 1), which is similar to the Skalak shape. The Cassini-based shape is a first analytical non-convex shape model of erythrocyte. In contrast to the Skalak and other experimental shapes, the Cassini model allows to represent DS in an explicit form, which gives an essential advantage in computing time.

For numerical modeling we choose the incident wavelength $\lambda = 476 \text{ nm}$, which corresponds the wavelength of 633 nm in water and in this wavelength we allows to ignore the absorption inside an erythrocyte. The refractive index of erythrocyte then is $n = 1.06$. In all the presented results the DSC and indicatrices are shown in the direction opposite to the incident direction ($\theta = 0^\circ$). All the particles have the same diameter $D = 6.3 \mu\text{m}$ and aspect ratio of 4:1. In Fig. 2 numerical results for DSC (12) versus scattering angle are presented for an incident angle $\theta = 135^\circ$. To give a better impression in Fig. 3 the same results are shown in a smaller range of scattered angles, which are of more interest for practical applications. From comparison one can see, that the scattering results for the disk-sphere and Cassini-based shapes demonstrate closer fitting to the results obtained for the Skalak shape. But while the disk shape fits better for smaller scattering angles, the Cassini shape fits better with increasing scattered angle. The spheroid seems to be the worst approximation for erythrocyte.

In Fig. 4 results for scattering indicatrices versus scattered angle are presented for the disk-sphere for different incidences. With increasing deviation from the axis of particles symmetry the amplitude of oscillations gets smaller, but the oscillations do not disappear at all. In Fig. 5 scattering indicatrices are presented for disk-sphere and oblate spheroid for side incidence ($\theta = 90^\circ$). One can see that for the spheroid oscillations are also present. We conclude that for other shapes the indicatrix behaves similar, but because of small amplitude of oscillations it could be difficult to measure them [6].

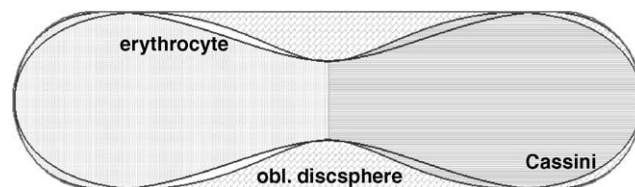


Fig. 1. Different erythrocyte shape models.

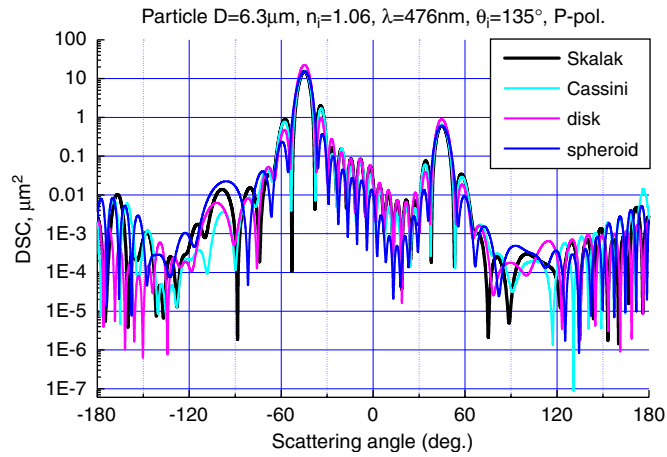


Fig. 2. DSC (12) versus scattering angle for different erythrocyte shapes are presented. Particles diameter $D = 6.3 \mu\text{m}$, P -polarized light, incident angle 135° .

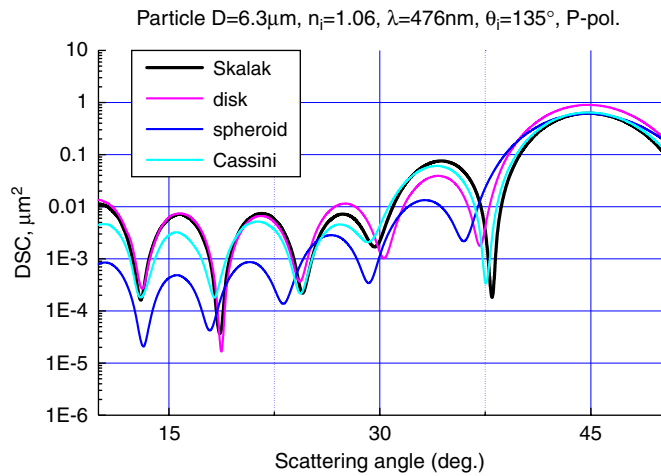


Fig. 3. For better overview the results of Fig. 2 are presented for the scattering angles range $10\text{--}50^\circ$. Particles diameter $D = 6.3 \mu\text{m}$, P -polarized light, incident angle 135° .

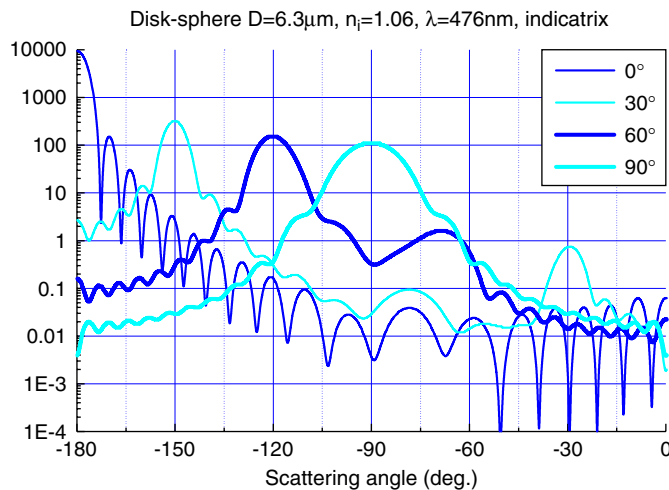


Fig. 4. Scattering indicatrices versus scattered angle are presented for disk-sphere shape for different incident angles, P -polarization.

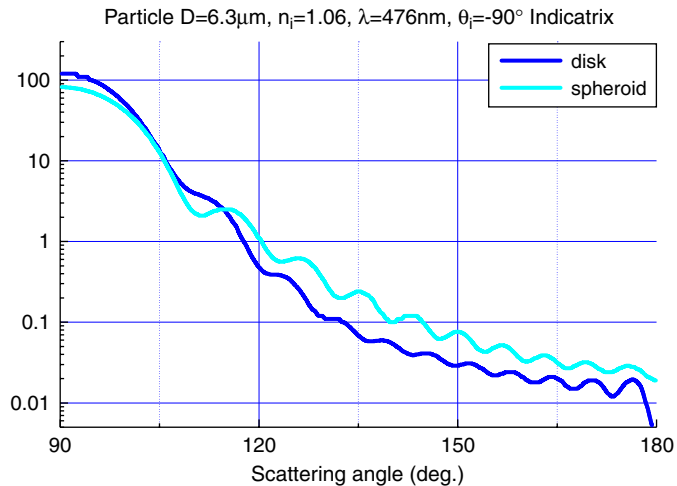


Fig. 5. Scattering indicatrices versus scattered angle are presented for disk-sphere and oblate spheroid shapes for incident angle of 90° , P -polarization.

4. Conclusion

In the paper the DSM has been applied to compare light scattering from different shapes of erythrocyte. The differential scattering cross sections and scattering indicatrices from different shape models of the erythrocyte have been presented. Further investigations of different erythrocyte shapes might be needed to find the optimal mathematical model when direct modeling of light scattering by real erythrocyte shape seems to be complicated.

References

- [1] Angelov B, Mladenov IM. On the geometry of red blood cell. Geometry, integrability and quantization. Varna: Bulgaria; 1999.
- [2] Skalak R, et al. Strain energy function of red blood cell membranes. *Biophys J* 1973;13:245.
- [3] Fung YC, Tsang WC, Patitucci P. High-resolution data on the geometry of red blood cells. *Biorheology* 1981;18:369.
- [4] Wriedt T, Hellmers J, Eremina E, Schuh R. Light scattering by the erythrocyte: comparison of different methods. *JQSRT* 2006; in print.
- [5] Lu JQ, Yang P, Hu X H. Simulations of light scattering from a biconcave red blood cell using the finite-difference time-domain method. *J Biomed Opt* 2005;10(2):024022.
- [6] Karlsson A, He JP, Swartling J, Andersson-Engels S. Numerical simulations of light scattering by red blood cells. *IEEE Trans Biomed Eng* 2005;52(1).
- [7] Yurkin MA, Semyanov KA, Tarasov PA, Chernyshev AV, Hoekstra AG, Maltsev VP. Experimental and theoretical study of light scattering by individual mature red blood cells with scanning flow cytometry and discrete dipole approximation. *Appl Opt* 2005;44(N25):5249.
- [8] Nilsson AMK, Alsholm P, Karlsson A, Andersson-Engels S. T-matrix computations of light scattering by red blood cells. *Appl Opt* 1998;3:2735.
- [9] Sveshnicov AG, Eremin YA. Numerical investigation of scattering problems on bodies of revolution by non-orthogonal series method. *Izv Vyssh Uchebn Zaved Radiofiz* 1980;23(8):580.
- [10] Y. Eremin, Orlov N, Sveshnikov, A. In: T. Wriedt, editor. *Generalized multipole techniques for electromagnetic and light scattering*: Amsterdam, Elsevier Science; 1999.p. 39.
- [11] Eremina E, Eremin Y, Wriedt T. Analysis of light scattering by different shape models of erythrocyte based on discrete sources method. *Opt Comm* 2005;244:15.
- [12] Maltsev VP. Scanning flow cytometry for individual particle analysis. *Rev Sci Instrum* 2000;71:243.
- [13] Colton D, Kress R. *Inverse acoustic and electromagnetic scattering theory*. Berlin: Springer; 1992.
- [14] Doicu A, Eremin Y, Wriedt T. *Acoustic and electromagnetic scattering analysis using discrete sources*. London: Academic Press; 2000.

- [15] Voevodyn V, Kuznetsov A. Matrices and calculations. Moscow: Science; 1982 [in Russian].
- [16] Maltsev VP, Semyanov KA. Characterisation of bio-particles from light scattering. Utrecht, Boston: VSP; 2004.
- [17] Bohren CF, Huffman DR. Absorption and scattering of light by small particles. New York: Wiley; 1983.
- [18] Hellmers J, Eremina E, Wriedt T. Simulation of light scattering by biconcave Cassini ovals using the null-field method with discrete sources. *J Opt A: Pure Appl Opt* 2006;8(1).